Materials and Design 191 (2020) 108652

Contents lists available at ScienceDirect

Materials and Design

journal homepage: www.elsevier.com/locate/matdes

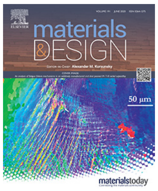

Microstructural and micromechanical assessment of aged ultra-fast sintered functionally graded iron/tungsten composites

S. Heuer [a],*, B.-S. Li [b], D.E.J. Armstrong [b], Y. Zayachuk [c,b], Ch. Linsmeier [a]

[a] *Forschungszentrum Jülich GmbH, Institut für Energie- und Klimaforschung - Plasmaphysik, Partner of the Trilateral Euregio Cluster (TEC), 52425 Jülich, Germany*
[b] *Department of Materials, University of Oxford, Parks Road, Oxford OX1 3PH, United Kingdom*
[c] *UK Atomic Energy Authority, Culham Science Centre, Abingdon, OX14 3DB, United Kingdom*

HIGHLIGHTS

- Fe/W composites aged at 300, 500, and 800 °C show fast precipitation of brittle intermetallics
- Via a rule of mixture, hardness and modulus of individual phases on the microscale are correlated to effective properties
- Interfaces between Fe and W volumes, studied via micro-cantilever bending, show very low toughness (K_{Ic} = 1.85 MPa $m^{0.5}$)

GRAPHICAL ABSTRACT

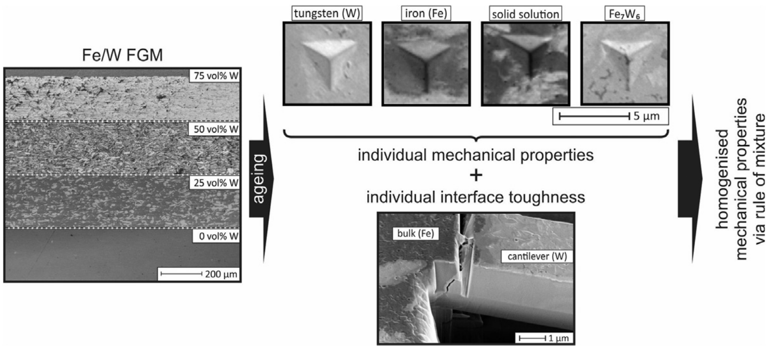

ARTICLE INFO

Article history:
Received 26 November 2019
Received in revised form 2 March 2020
Accepted 16 March 2020
Available online 21 March 2020

Keywords:
Tungsten-steel composites
Functionally graded materials (FGM)
Nanoindentation
Micro-cantilever bending
Multi-scale characterization
Nuclear fusion
DEMO
First wall

ABSTRACT

Functionally graded (FG) iron/tungsten (Fe/W) composites are considered for stress-relieving interlayers in tungsten-steel joints, required in future fusion reactors. The macroscopic gradation of the two materials allows relaxation of thermally-induced stresses and hence extend the lifetime of the cyclic-loaded dissimilar materials joints. While many properties, e.g. thermal expansion and strength, of the as-manufactured Fe/W composites are promising with respect to the anticipated application, the temperature-induced microstructural changes and their effect on the material properties remain largely unexplored. Given that the thermodynamic system of Fe—W contains two types of intermetallic phases, understanding the microstructural changes in the FG Fe/W composites is crucial for long-term operation of fusion reactors.

In the present work, the microstructure of ultra-fast sintered Fe/W composites containing 50 and 75 vol% tungsten is studied via electron microscopy (SEM) and X-ray diffraction (XRD) in as-manufactured and thermal aged conditions (300, 500, and 800 °C for up to 72 h). The hardness and modulus of selected composites are measured via nanoindentation, and the fracture toughness of the Fe—W interfaces is tested via notched micro-cantilever bending tests. The results from microstructural and micromechanical analyses are discussed, and the materials are evaluated for their application in fusion reactors based on the microstructure-to-property relationship.

---

* Corresponding author.
E-mail address: s.heuer@fz-juelich.de (S. Heuer).

https://doi.org/10.1016/j.matdes.2020.108652
0264-1275/

1. Introduction

Future fusion reactors beyond ITER are foreseen to feature a first wall that composes of a tungsten armour layer and a steel structure, both as yet undefinedly bonded to one another. A direct tungsten-steel joint, proposed in current engineering design studies [1–3], is accompanied by discontinuously changing material properties, e.g. the coefficient of thermal expansion transitions from 12.0×10^{-6} K^{-1} of steel to 4.4×10^{-6} K^{-1} of tungsten at room temperature. As a consequence, after joining and during reactor operation, significant thermally-induced stresses could develop at the macroscopic tungsten-steel interface, causing premature failure of first wall joints [4–6]. Hence, implementing functionally graded (FG) layers in the joint may extend its lifetime.

FG materials compose of at least two constituents, which are microscopically arranged in a specific manner, so that a uni- or multi-directional gradation of the constituents can be achieved. A simple example is a plate that composes of iron (Fe) at the bottom and of tungsten (W) at the top, with a linear gradation of the constituents across the thickness of the plate. The expected property gradation with the variation is desired for interlayers implemented in dissimilar material joints because the thermally-induced macro-stresses and strains are dissipated from a discrete interface into a larger volume, hence lowering the stress peaks [5,7,8].

Finite element analyses have shown that the implementation of FG Fe/W interlayers in tungsten-steel joints in the first wall of future fusion reactors may produce a noticeable positive effect when the thickness of the FG layer is of the order of one millimetre [5]. This boundary condition suggests following a powder metallurgical route for fabricating the FG layers, because physical vapour deposition, chemical vapour deposition or electro plating, all of which can be used for the production of perfectly graded deposits, only make thinner layers. Powder metallurgic composites, however, only approximate FG materials by arranging microscopic particles of at least two constituents in a varying ratio across an interlayer. The structure is not ideal but always exhibits discrete volumes of the pure constituents on the microscale. Despite this imperfection, producing graded Fe/W composites by means of powder metallurgy has proven successful [9–14], and particularly vacuum plasma spraying (VPS), atmospheric plasma spraying (APS) and electro discharge sintering (EDS) are promising techniques. An exemplary micrograph of an FG Fe/W composite made by EDS is shown in Fig. 1.

For composite materials such as the graded layer of Fig. 1, many rules of mixture already exist for estimating the material properties. An overview of frequently applied rules for the calculation of the CTE is discussed in [15]. Despite the heterogeneous microstructure of the graded Fe/W composite, the idealised linear rule of mixture, Eq. (1), has successfully reflected the graded CTE of this material [13].

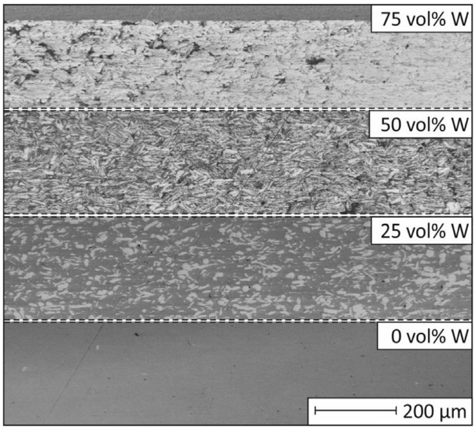

Fig. 1. Exemplary micrograph of FG Fe/W composites made by EDS [13].

$$p(f_W) = f_W\, p_W + (1-f_W)\, p_{Fe} \quad (1)$$

In the shown generalised form, p represents any material property as a function of tungsten content f_W, and the parental material properties p_i. In contrast to this ideal representation, the measured thermal conductivity and yield strength do not correspond to the weighted mean properties of the parental materials [13]. Two aspects are considered to be important for this behaviour. First, high density of interfaces including constituent boundaries (indicated as *Fe—W* in the following), particle-to-particle boundaries, and grain boundaries within the Fe/W matrix can affect thermo-physical and mechanical properties. Interfaces act as thermal barriers, as described by the Hasselman-Johnson model [16], and impede dislocation motion. Secondly, Fe—W interfaces are favourable nucleation sites for intermetallic phases, Fe_7W_6 and Fe_2W, according to the thermodynamic iron-tungsten phase diagram [17]. Particularly Fe_7W_6 is reported to exhibit a complex unit cell [18], which has limited slip systems. If present, Fe_7W_6 will increase the overall strength but also reduce ductility significantly, hence is not desired in the graded structure.

Aiming at a more elaborated description of FG materials' properties than using the existing rule of mixture, several studies have been carried out in recent years for different material systems and microstructures. These studies may be separated into two categories. The first category considers FG materials as stacks of discrete sublayer continua, whose properties are described as *effective properties* (individual constituents are neglected). The second category considers individual constituents on the microscale and calculates the *homogenised properties* using different homogenisation models. Studying effective properties of sublayers is usually faster and does not rely on simplified assumptions like homogenisation. However, the respective testing techniques do not yield information about material properties and responses at the microstructural level. Simple and sufficiently accurate methods for the determination of effective mechanical properties of graded materials were for instance presented by Koohbor et al. [19]. In their study, an experimental method using tensile and four-point bending tests has been developed to determine the through-thickness modulus of graded structures. Measuring strains on two sides of FG Ti/TiB samples and applying a one-dimension classical laminate theory they calculated the beam stiffness and, based on an inverse approach, the elastic modulus. Other inverse methods presented in [20–22] are more complex and require high computational power. Techniques for the direct measurement of effective elastic properties of single FG material sublayers were presented by Butcher et al. [23], who carried out ultrasound testing, Nakamura et al. and Branch et al., who used (instrumented) micro-indentation [20,24], and Ruigang et al., who combined previous techniques with three point bending tests, characterising $Si3N_4$/BN composites [25]. Methods for measuring fracture toughness [26,27] and crack behaviour in graded materials with a crack parallel and transversal to the gradation direction were presented by several studies [28–33]. In these, the FG structures were analysed as a whole, hence fracture behaviour at microstructural level is only vaguely discussed.

While many studies focus on the measurement of effective material properties of graded materials, only few discussed FG Fe/W or steel/W layers. To date, direct measurement of hardness or elastic modulus are only reported by Qu et al. [11,34], Matejicek and Boldyryeva [35], Weber et al. [10], Heuer et al. [13,14], and Vassen et al. [36]. Although similar types of FG materials were tested in these studies, the modulus and hardness strongly depend on the FG composite fabrication and testing technique. For example, Qu et al. have prepared graded steel/W layers by vacuum plasma spraying and resistance sintering under ultra high pressure and measured the effective Vickers hardness of 50 vol % W layers to be 2.7 GPa and 0.5 GPa, respectively. Based on the incremental hole drilling method, Vassen et al. computed the elastic modulus of the vacuum plasma sprayed layer to be 235–270 GPa [36], whereas Matejicek et al. measured only 57 GPa for an atmospherically plasma sprayed layer containing 50 vol% W. In a similar material, Heuer et al. measured a modulus of 170–200 GPa [14], and in 50 vol% W composites fabricated by EDS, the effective modulus was measured to be 230 GPa [13]. The variations indicate that comparing the mechanical properties of Fe/W composites can be difficult as the results are heavily influenced by the processing methods and the consequential microstructural features.

In contrast to testing material properties from single sublayers, several authors have focussed on the material properties of individual constituents and used them to calculate homogenised properties for specific FG composite mixtures. Akbarzadeh et al. have given an overview of different micromechanical models on the structural response of FG layers [37]. Earlier, Weissenbek et al. studied the elastic-plastic deformation of graded Ni/Al_2O_3 structures from thermal and mechanical loads. Their numerical results are compared with a rule of mixture, the mean-field approach involving an incremental Mori-Tanaka analysis, and experimental results [38]. The Mori-Tanaka model was also successfully implemented in the comparison of modelled properties of several functionally graded materials, and was experimentally validated by Yu and Kidane [39]. Schmauder et al. used a so-called *matricity factor* to describe the through-thickness properties of graded Al/TiO_2 structures [40].

Above micromechanical homogenisation approaches focus on other material systems than the Fe/W composites and often rely on literature data from commercially available bulk materials. For the present Fe/W composites, using material properties from literature is less accurate because the fabrication process will strongly affect the properties of the individual constituents. Hence, for composites similar to the present Fe/W structures (steel/W made by spark plasma sintering and hot pressing), Matejicek et al. have studied the modulus and hardness of steel, W and Fe_7W_6 via nanoindentation [41,42]. Additionally, Koller et al. have studied the relationship of microstructure and effective modulus of the spark plasma sintered material via resonant ultrasound spectroscopy and finite element analyses [43]. According to their study, the bonding quality of neighbouring volumes plays an important role for the effective modulus, which, in consequence, is important for the calculation of homogenised properties in future studies.

In summary, extensive studies have been carried out on measuring effective material properties or homogenised properties of graded materials. Only few studies compared the measured effective properties with results the from homogenisation, and none of these were conducted on the Fe/W system. Moreover, most studies focused on as-manufactured FG material. Considering that the materials will be applied in a high temperature environment, morphological changes of the microstructure of Fe/W or steel/W composites in general have not received due attention. Only the precipitation of intermetallic phases during composite production and to some extend after short annealing has been described in some studies. In this context, Matejicek et al. and Koller et al. used spark plasma sintering with several sintering temperatures (1100 to 1400 °C) and times (2 and 30 min) for the consolidation of mixed steel/W powders [41,43]. After short sintering at 1100 °C, continuous seams of Fe_7W_6 at the steel-W interfaces were found, which increase in thickness with higher sintering temperatures. At 1400 °C after sintering for 30 min, all steel and most of the tungsten volumes are replaced by the intermetallic phase. Similar microstructural changes are described for W/steel composites hot pressed at 2000 °C [42]. While intermetallic seams of Fe_2W at the interfaces after hot pressing were circa 3.5 μm thick, annealing for 4 h at 1000 °C caused an increase by 12 to 59%. In contrast to these observations, no morphological changes are reported in [10], where vacuum plasma sprayed W/steel composites are annealed at temperatures up to 1000 °C for one hour. Despite these studies, work systematically investigating the microstructure morphology of Fe/W or steel/W composites after extended heat treatment durations at several temperatures does not exist. For the successful implementation of FG Fe/W composites in fusion reactors, a better understanding of the relationship between the microstructural features and the effective material properties is required. In this manuscript, homogenised and effective mechanical properties of aged Fe/W composites are compared for the first time. The microstructures of ultrafast sintered Fe/W composites are characterised before and after ageing to investigate their thermal stability. Then, nanoindentation is used to measure the effective modulus and hardness of the composites, and also from the individual constituents. The homogenised properties are estimated using a combination of linear rule of mixture, quantitative image analyses, and properties from individual constituents, and are compared with micro-indentation results. Lastly, fracture behaviour of the Fe—W interfaces is measured using chevron-notched micro-cantilever bending tests. Transmission electron microscopy (TEM) is used to provide detailed chemical profile along the crack path.

2. Materials and methods

2.1. Materials

Composites studied in this manuscript were made by electro discharge sintering (EDS). EDS consolidates lose powders at atmosphere within milliseconds by simultaneously guiding a high electric current (≤400 kA) through the powder and uniaxially compressing it (≤388 MPa). Details about the fabrication technique may be found elsewhere [13,44].

Fabrication of Fe/W composites for the present study follows processing conditions from [13], in which materials containing 0, 25, 50 and 75 vol% W were produced. Here, a subset of these composites only containing greater W fractions (50 and 75 vol% W, indicated as *50* W and *75* W in the following context) is studied. For their fabrication, commercially available gas atomized Fe raw powder (Goodfellow, England) of average size 6–8 μm and W raw powder (Umicore, Belgium) of average particle size 11–13 μm made by hydrogen reduction of tungsten trioxide were used. Fe/W powder mixtures containing 50 and 75 vol% W were ball-mixed for 8 and 4 h, respectively, to adjust a fine distribution of discrete Fe and W volumes within powder particles before sintering. EDS was carried out with ball-mixed powders and the highest energy and pressure possible, i.e. 400 kA and 388 MPa. Measuring the actual sintering temperature is not possible with EDS due to the closed system and the short process time. All relevant parameters are summarised in Table 1. Sintering produced cylindrical samples of 3 mm height and 19 mm diameter. The theoretical density of all samples reaches ca. 97% [13]. Overview images of the microstructures of these composites in the as-sintered condition are represented by the upper half of the FG Fe/W layer, Fig. 1.

2.2. Ageing

A subset of sintered Fe/W composites was subjected to heat treatments to mimic reactor heat loads on the first wall. Heat treatments were carried out in a vacuum furnace at a pressure of 5.5×10^{-5} mbar, under the following conditions:

- 800 °C for 24 h
- 500 °C for 24 h
- 300 °C for 72 h

Given an α-γ phase transition temperature of the steel pursued for fusion applications of ca. 820 °C [45,46], the upper temperature limit of steel-containing parts of the first wall is approximately 800 °C. This temperature will have to be maintained for a small fraction of the anticipated five years lifetime of the first wall only, i.e. for few hours during first wall assembly and during fusion plasma instabilities. According to finite element analyses, it is estimated that the temperature within

Table 1
Process parameters used for the fabrication of Fe/W composites by ball-mixing and subsequent electro discharge sintering.

Material indicator	Particle size before mixing		Mixing ratio	Ball-mixing duration	Ball-powder ratio	Mixing speed	Sintering discharge	Mechanical pressure	Powder mass	Final sample size (height × diam.)
	µm		vol% Fe/vol% W	h	g/g	rpm	kA	MPa	g	mm × mm
	Fe	W								
50 W	6–8	11–13	1/1	8	5/1	200	400	388	11.56	3 × 19
75 W	6–8	11–13	1/3	4	5/1	200	400	388	13.99	3 × 19

the tungsten-steel joint of the first wall during reactor operation is around 500 °C (under the assumption described in [5]). If water is chosen as the coolant of the first wall, a cooling temperature of 300°C is assumed in current reactor design studies [1,2], and will be the lowermost temperature that Fe/W composites experience in operation. Ageing for an extended duration (72 h) was selected for 300 °C because this temperature will have to be endured longer than plasma pulse-generated higher temperatures, i.e. during plasma pulses and in between. Although the thermal ageing time chosen here is much shorter than the first wall lifetime, it should still provide insights for initial ageing experiments.

2.3. Microstructural characterization

For microstructural characterization, approximately one third of the sample height was removed by grinding, followed by polishing until the surface exhibits a mirror finish. Microstructural characterization was carried out using a field emission gun scanning electron microscope (FEG-SEM) (*Merlin*, *Carl Zeiss*, Germany) equipped with both secondary electron (SE) and electron backscatter diffraction (EBSD) detector. At least five back scatter electron images (for better composition contrast) taken at 500× optical magnification were used for quantitative composition analysis. For chemical analysis, another FEG-SEM equipped with an energy dispersive X-ray (EDX) detector was used. X-ray diffraction (XRD) was applied for the investigation of different constituents present in Fe/W composites. A *Discover D8* diffractometer (*Bruker*, Germany) equipped with a Cu X-ray source was used for these studies. A *JEOL-2100 LaB*$_6$ transmission electron microscope (TEM) (*JEOL*, Japan) equipped with an EDX detector (*EDAX*, USA) was used to carry out the crack path chemical analysis from the fractured cantilever.

2.4. Micromechanical characterization

The hardness, modulus and Fe—W interfacial fracture toughness were measured using instrumented indentation and micro-cantilever bending tests.

A *G200 Nanoindenter* (*KLA*, USA) equipped with a fully-calibrated diamond Berkovich tip was used for the indentation tests. All indents were carried out using continuous stiffness measurement (CSM) with testing parameters given in Table 2. Arrays of 5 × 5 indents with spacing of approximately 15–20 µm were made in regions without significant surface pores. Some indents tested a mixture of constituents, while some tested either pure Fe, pure Fe_7W_6, or pure W. Average modulus and hardness of each indent were calculated using depth between 250 and 450 nm. In preceding experiments with indentation depth ranging from 200 to 2000 nm, 500 nm nominal depth was found to allow testing of individual constituents, and also provide enough sampling volume to neglect any surface effects. Here, *modulus* and *hardness* refer to indents that only tested single constituents, and *effective modulus* and *effective hardness* refer to the average values calculated from a 5 × 5 indentation array. For comparison, micro-indentation with a Vickers indenter was carried out. 10 randomly selected positions were tested in each composite with a load of 0.5 kgf (HV0.5).

For assessment of the Fe—W interfacial fracture toughness, micro-cantilevers were prepared in an as-sintered 50 W composite and in a 75 W composite aged at 800 °C for 24 h using a focussed ion beam (FIB), following procedures developed by di Maio and Roberts [47]. The cantilevers were precisely positioned on the Fe—W interface, with most of the cantilever residing within the W volume. An example of a cantilever is given in Fig. 2. A chevron-type notch was prepared at the Fe—W interface, as shown in Fig. 2 b), then the cantilever was displaced near the free end using a nanoindenter until complete fracture. The chevron-notch design, due to its sharp apex and increasing crack front, forces fracture to initiate at the interface and propagates stably, hence improving the interfacial fracture toughness measurement. This technique has been evaluated on tungsten alloy and silicon and was shown to be specifically suitable for the toughness calculation of brittle materials [48]. Here, we also expect the interface to be fairly brittle, based on previous macroscopic bending tests [13].

Table 2
Nanoindentation boundary conditions.

Parameter	Value
Depth limit	500 nm
Frequency target	42.0 Hz
Harmonic displacement target	2.0 nm
Strain rate target	0.05 s^{-1}
Peak hold time	10 s

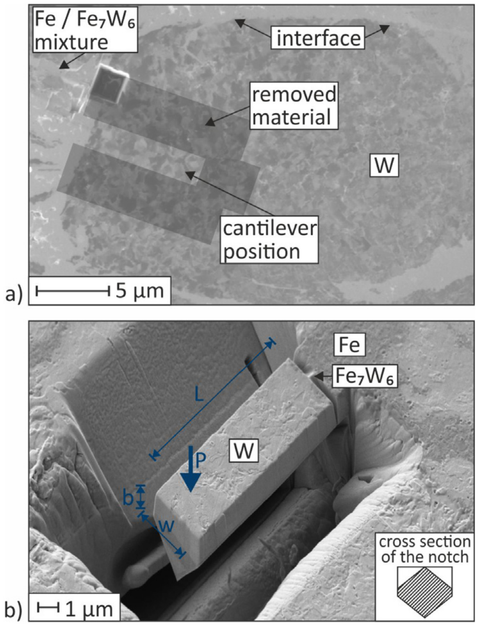

Fig. 2. Exemplary cantilever used for interface characterization. a) Position of cantilevers in W volumes, b) chevron-type notched cantilever before bending.

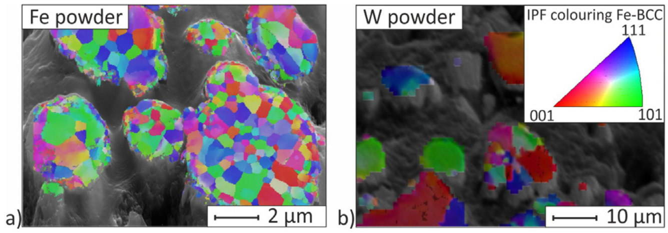

Fig. 3. SE images of raw Fe and W powders with inverse pole figures from EBSD analyses. a) Fe 6–8 µm, b) W 11–13 µm.

Bending of the micro-cantilevers was carried out using a *G200 Nanoindenter* with a blunt Berkovich tip. The cantilevers were firstly scanned using very low contact force (~1 μN) to produce a topological image for precise loading. Tests were carried out in load-controlled mode, using a constant loading rate of 10 μN s^{-1}. Using the load at unstable fracture, P_c, and the stress intensity factor (SIF), Y_{min}, the interfacial fracture toughness K_{Ic} was calculated using Eq. (2).

$$K_{Ic} = P_c \frac{Y_{min}}{b\sqrt{w}} \tag{2}$$

Parameters b and w are indicated in Fig. 2. Load at unstable fracture, P_c, was chosen when a significant displacement jump (>500 nm) was observed. The non-dimensional SIF Y is calculated via the finite element software ABAQUS CAE 6.14 (Dassault Systems, France), using the contour integral analysis. In the analysis, crack length, crack front and crack direction are defined, then the contour integral analysis computes a J-integral at each node along the crack front. Assuming plane-strain condition, the J-integrals are converted to the non-dimensional SIF. The crack growth is modelled incrementally, and the Y value at each crack length is plotted against the crack length. Due to the sharp apex and increasing crack front provided by the chevron geometry, a transition between stable and unstable crack growth is expected when the crack reaches the critical crack length α_c (at which point Y reaches Y_{min}). For more details of the parameter Y_{min} and the modelling (e.g. mesh type, boundary conditions, etc.) the reader is referred to [48].

3. Results and discussion

3.1. Fe/W microstructures before and after ageing

Fe particles (6–8 µm) are spherically shaped, W powder (11–13 µm) composes of irregular particles that form stable agglomerates [13]. Exemplary cross sections of the used raw Fe and W powder, superposed with out-of-plane inverse pole figures (IPF-Z) from EBSD analyses, are shown in Fig. 3 a) and b). For these analyses, samples were embedded in duroplast and then first ground with SiC paper for 3–5 min at several grit sizes (P400, P600, P800, P1200, P2000), followed by polishing with diamond paste containing 6, 3, and 1 µm diamond particles for 3 min each, and with colloidal silica (0.25 µm) for 30 s. From the inverse pole figures, both Fe and W particles compose of very fine grains.

During ball-mixing, repetitive cold working and fracturing of particles caused particle coarsening and formation of lamellar Fe/W structures, shown in Fig. 4. According to XRD, no alloying of Fe and W occurred [13].

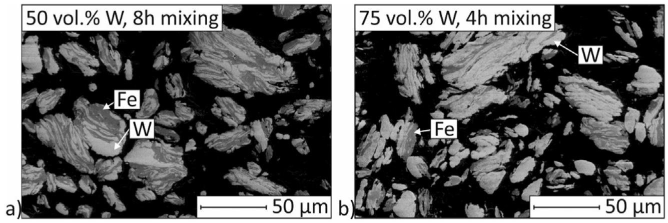

Fig. 4. Powders after ball-mixing. a) 50 W after 8 h mixing, b) 75 W after 4 h mixing [13].

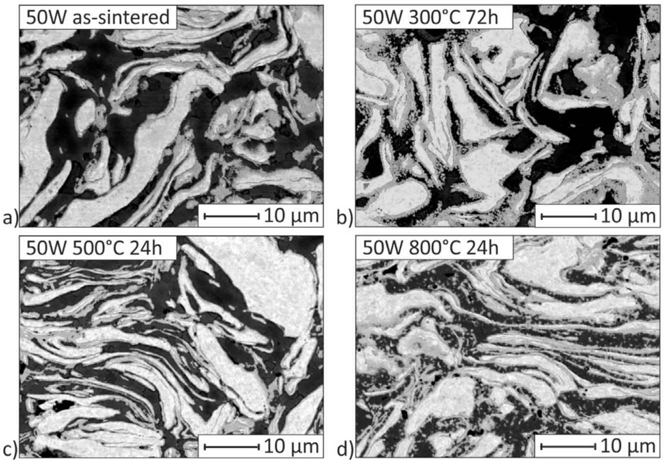

Fig. 5. Sintered 50 W composites. a) as-sintered, b) aged 300 °C, 72 h, c) aged 500 °C, 24 h, d) aged 800 °C, 24 h.

Cross sections of as-sintered and heat-treated 50 W and 75 W composites are presented in Figs. 5 and 6. The lamellar structure of the ball-mixed particles is preserved in the composites after sintering. Dark field TEM images, shown for an as-sintered 50 W composite in Fig. 7, indicate that the fine grain size of the raw Fe powder is preserved in the sintered composites. The grain size of W was further reduced and a high density of dislocations is observed.

In all composite overview images, Figs. 5 and 6, a distinct mid-grey region is observed in between the Fe (black) and W (light grey) volumes. These mid-grey regions are limited in as-sintered composites, but become larger after ageing, which agrees with observations for spark plasma sintered W/steel composites after short annealing [41,43]. Exemplary EDX measurements indicate that their Fe/W ratio equals approximately 1/1, suggesting they represent the intermetallic phase Fe_7W_6. This is in good agreement with XRD results, shown in Fig. 8. For all conditions, XRD identifies a combination of the phases W, Fe, solid solution ($Fe_{0.95}W_{0.05}$), and Fe_7W_6. Fe_2W, however, is not found in the samples after any ageing condition.

Based on the identification of the constituents, quantitative image analysis was used to calculate the constituent portions in the composites before and after ageing. The results are given in Table 3. The solid solution portion is not quantified because the contrast is too low to distinguish from the pure Fe, hence the solid solution and Fe volumes are combined. The effect of ageing on the Fe_7W_6 portion is additionally

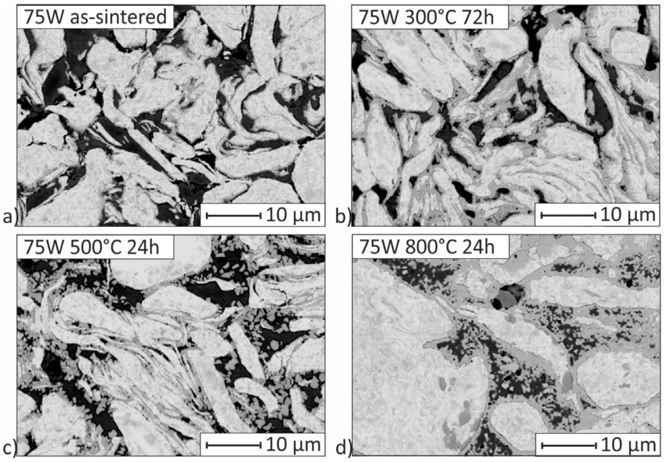

Fig. 6. Sintered 75 W composites. a) as-sintered, b) aged at 300 °C for 72 h, c) aged at 500 °C for 24 h, d) aged at 800 °C for 24 h.

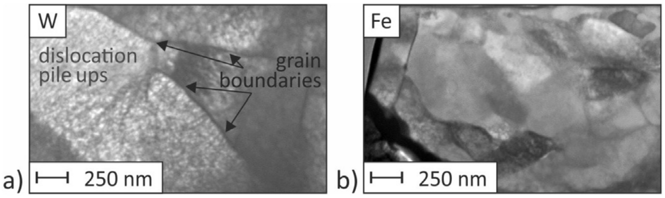

Fig. 7. Dark field TEM images of Fe and W volumes in an as-sintered 50 W composite.

visualized in Fig. 9. Based on earlier work by Delesse [49], for a statistically isotropic structure, area fractions may be representative of the volume fractions. According to quantitative image analysis, the portion of intermetallic phase in 50 W and 75 W composites is already high after sintering (~22 vol%) and increases to >30 vol% after 72 h ageing at 300 °C. Ageing at 500 °C causes less precipitation due to the shorter ageing time. It is assumed that the Fe_7W_6 precipitation seams at the Fe—W interfaces act as diffusion barriers with comparably low Fe and W diffusion rates at 300 and 500 °C. If diffusion of Fe and/or W through the intermetallic precipitate seam is similar at 300 °C and 500 °C, then the applied time (72 vs 24 h) has a greater effect on the amount of further Fe_7W_6 precipitation than temperature. At 800 °C the higher diffusion rates cause further increase of Fe_7W_6 to 37 vol% within 24 h. The rate of microstructural change seems to be independent from the Fe/W ratio of the composites as indicated by Fig. 9.

The precipitation of Fe_7W_6 is expected to play an effect on the material properties of the composites compared to the as-sintered condition. For engineering applications, this change has to be quantified because even if precipitation can be suppressed during composite fabrication, Fe_7W_6 will still form in a short amount of time compared to the expected lifetime of the first wall. Alloying significant amounts of nickel (ca. 30 wt%) into steel would suppress the precipitation of intermetallics [50], but adding nickel in fusion reactors is undesirable as it forms the highly radioactive cobalt-60. The replacement of Fe in FG layers by actual fusion-relevant steels is not expected to be much more thermodynamically stable. Therefore, the constituents identified from quantitative image analysis are characterised micromechanically in the following context and and homogenised properties are calculated from the results, which are compared with effective material properties.

3.2. Modulus and nanohardness of Fe/W composites

A subset of Fe/W composites subjected to fusion-relevant heat treatments (as-sintered, 300 °C 72 h, and 800 °C 24 h) are investigated via nanoindentation. Here, modulus and hardness of the individual constituents are firstly discussed, then the results are compared with the effective properties.

Table 3
Shares of the individual constituents in 50 W and 75 W composites before and after ageing according to quantitative image analysis. The results represent the average composition of five images; errors represent the standard deviation.

Sample	composition [area%]		
	W	Fe_7W_6	Fe
50 vol% W			
as-sintered	34 ± 1.1	24 ± 1.1	43 ± 1.4
300 °C, 72 h	31.5 ± 3.2	32 ± 5.0	36.5 ± 1.8
500 °C, 24 h	34.2 ± 1.2	26.2 ± 2.0	39.6 ± 1.9
800 °C, 24 h	32.3 ± 3.1	36.8 ± 2.4	31 ± 1.6
75 vol% W			
as-sintered	63.2 ± 2.5	21.4 ± 9.8	15.4 ± 8.0
300 °C, 72 h	55.8 ± 3.3	30.2 ± 4.8	14 ± 4.2
500 °C, 24 h	62 ± 3.0	22.6 ± 4.7	15.4 ± 2.0
800 °C, 24 h	55 ± 1.9	37.3 ± 3.6	7.8 ± 1.8

3.2.1. Properties of individual constituents

The Fe/W composites consist of Fe, W, Fe_7W_6, and solid solution in different portions. Exemplary images of indented individual constituents are shown in Fig. 10 to provide an estimate of the indentation size and surrounding volume. The indentation depth and size were selected so that indents are not larger than the volume of individual constituents in many cases. Modulus and hardness of the individual constituents measured in different samples are compared in Fig. 11 and summarised Table 4. For a more complete comparison, measured properties of the Fe and W raw powder, and results taken from literature [41] are added to Fig. 11 and Table 4. Whilst indents on pure W volumes succeeded in all composites, indents on pure Fe, solid solution and Fe_7W_6 are less successful due to the constituents' smaller volumes. Fe was only successfully tested in the 50 W composites, and Fe_7W_6 only in the 75 W composites. Hence, only modulus and hardness of W are compared across the different Fe/W composites. Other constituents are compared with respect to their different heat treatment conditions.

Fig. 11a shows a higher W modulus from the 75 W composites compared to the 50 W composites (430 GPa vs. 380 GPa). This is due to the contribution of softer constituents surrounding the W indents. In the 50 W composites, the larger volume fraction of the softer constituents attributes to the lower measured W moduli. Nevertheless, most measured moduli are in good agreement with results from literatures [41,43,46,51]. Only the measured modulus of W raw powder and of Fe raw powder are exceptionally low. This is because the powder particles were embedded in a compliant duroplast, hence affecting measuring the moduli. Fig. 11a also shows that heat treatments have no significant influence on the modulus of any of the individual constituents, only affecting their portions in the composites.

The hardness of the individual constituents are shown in Fig. 11a. The hardness of W is approximately 11.8 GPa, which is comparable to the results reported by [41] and is approximately twice the hardness

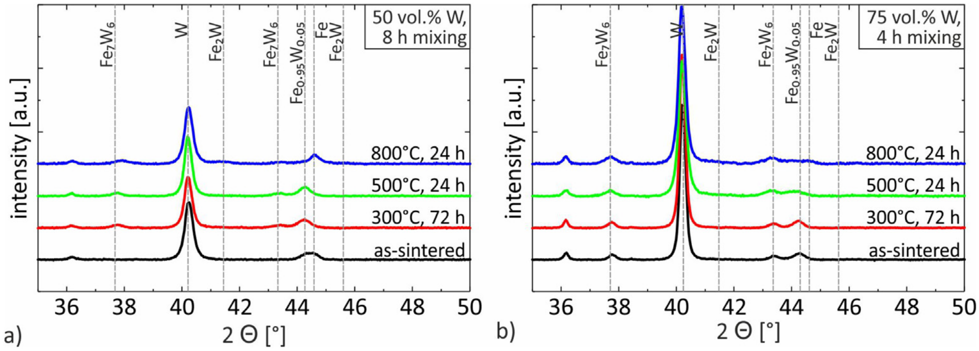

Fig. 8. Diffractograms of 50 W and 75 W composites in as-sintered and aged condition. a) 50 W composites, b) 75 W composites.

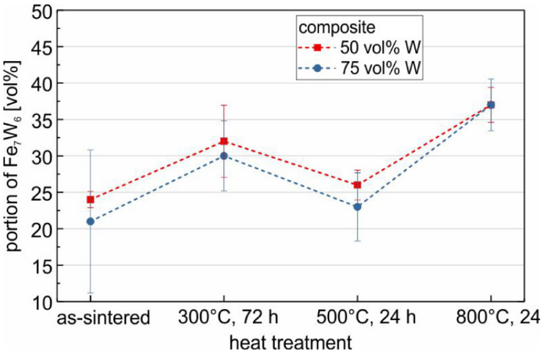

Fig. 9. Portion of the intermetallic phase Fe_7W_6 in 50 W and 75 W composites before and after ageing according to quantitative image analysis.

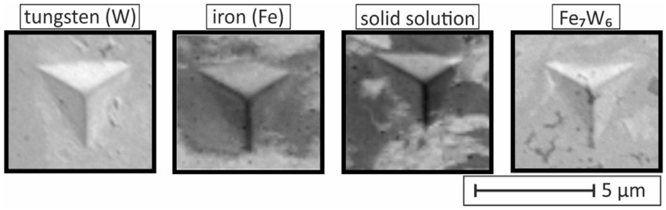

Fig. 10. Nanoindents in individual constituents present in Fe/W composites.

measured from single crystal W [52]. No significant differences for the W hardness are observed from different composites and powder. The hardness of Fe in as-sintered 50 W composites is around 5 GPa, which is also significantly higher than the hardness of single crystal Fe ranging from 2.2 to 4.1 GPa [53].

The high hardness of the constituents is caused by the fine grain size of the raw powder and by the severe plastic deformation during ball-mixing. As evident from TEM images in Fig. 7, fine grains and high dislocation densities are retained after sintering. In [54], the dislocation density in cold rolled tungsten increased heavily above 350% deformation and reached $9 \times 10^{(14)}\ m^{(-2)}$ at 400% deformation. Similar orders of magnitude may be expected in the W volumes of the present material.

The hardness of Fe_7W_6 is 17.2 GPa. This is approximately 23% lower than values from literature [41], but still 1.5 times higher than the measured W hardness.

Ageing does not change the hardness of any of the constituents studied here, which corresponds to the modulus measurements.

The very high hardness of W and Fe_7W_6 may contribute to the brittle failure of Fe/W composites observed in macroscopic fracture toughness and bending tests [13,55], but for a better understanding of the failure mechanism, the interfacial strength also needs to be investigated.

3.2.2. Homogenised Fe/W properties before and after ageing

Homogenised material properties of the composites are calculated to study the relationship between individual constituent properties and bulk properties of ideal Fe/W composites. If bridging the properties from individual constituents to the bulk composite is possible via a simple model such as the linear rule of mixture, then results from micromechanical testing can provide estimation of material properties of graded Fe/W composites. This would reduce the required amount of work for characterization of the heterogeneous material compared to measuring the mechanical properties of each sublayer of the graded material. Moreover, the relationship between properties from individual constituents and bulk properties can be used to provide modelling parameters for FG Fe/W materials in finite element analyses.

Results of homogenised modulus and hardness calculation for the composites before and after ageing are presented in Fig. 12 a) and b). They were based on the linear rule of mixture, quantitative image analysis, and properties from individual constituents. Results of effective composite properties from nanoindentation arrays and from micro-hardness measurement are also shown in Fig. 12. The effective composite properties measured by nanoindentation show large error bars due to the random sampling of constituents (Fe, W, solid solution, Fe_7W_6). Despite the measurement uncertainties, the modulus and hardness of the 75 W composites are both systematically higher compared to the results from the 50 W composites.

The effective modulus of all 50 W composites measured by nanoindentation agrees well with the homogenised value calculated from the rule of mixture. In contrast, the measured homogenised modulus of all 75 W composites studied here is systematically 10–12% higher than the calculation suggests (430 vs. 385 GPa). This difference is likely because no contact area correction was carried out post indentation, which is suggested if surface pile-up is significant [56]. Here, pile-up is larger in the 75 W than in the 50 W composites because the tungsten volumes are more dominant. The slender Fe—W structures of the 50 W composites allows a larger contribution of elastic deformation in iron around indents, hence the pileup effect on modulus is less pronounced. Ageing is found to have an insignificant influence on the effective modulus. While an increase of the Fe_7W_6 portion with ageing can be clearly seen via the quantitative image analyses, the effect on the effective modulus is covered in Fig. 12 a) by the large scattering.

Homogenised hardness, shown in Fig. 12 b), are in good agreement with effective hardness measured via nanoindentation and also reflect

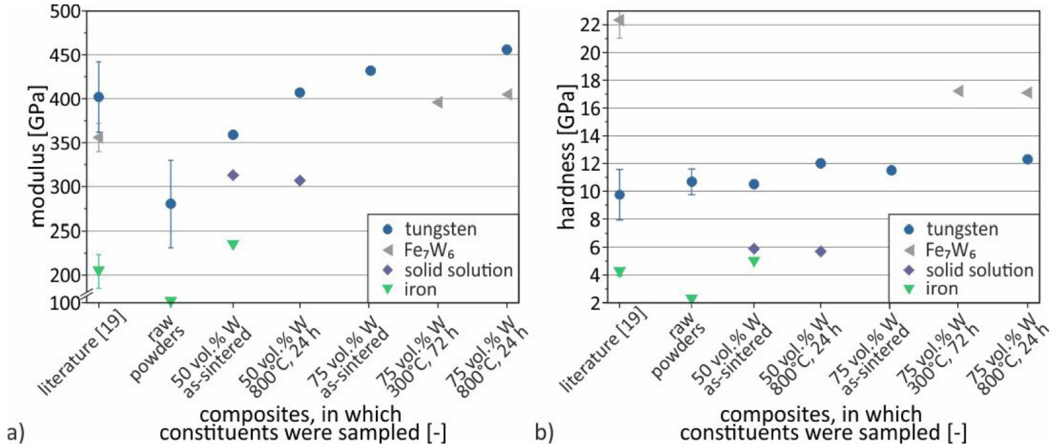

Fig. 11. Modulus (a) and hardness (b) of individual constituents measured in raw powders, in as-sintered composites, and after ageing.

Table 4
Mean modulus and hardness of individual constituents present in Fe/W composites. Errors represent the standard deviation of the results presented in Fig. 11.

Constituent	Modulus literature data [41]	Mean modulus measured	Hardness literature data [41]	Mean hardness measured
	(GPa)	(GPa)	(GPa)	(GPa)
Tungsten	402 ± 40	410 ± 32	9.8 ± 1.5	11.8 ± 0.6
Fe_7W_6	356 ± 16	400 ± 5	22.3 ± 1.3	17.2 ± 0.1
Solid solution	–	310 ± 3	–	5.8 ± 0.1
Fe (steel in [41])	205 ± 19	235	4.2 ± 0.2	5

ageing-induced microstructural changes. Only the 75 W composite aged at 300 °C for 72 h yields exceptionally high effective hardness compared to the other composites, close to the hardness of pure Fe_7W_6. It is possible that the number of indents was not sufficient enough for statistical representation of the homogenised properties in this composite. The change of material properties with ageing is expressed by hardness, but not by modulus measurements because the modulus of Fe_7W_6 is in between the moduli of Fe and W, whereas the hardness is much higher than that of both pure metals. Comparing effective nanohardness results with micro-hardness results, micro-hardness results are much lower, and they agree well with results presented by Qu et al. measured for vacuum plasma sprayed steel/W composites [34]. With nanoindentation, due to its fine volume, it is less likely that pores were sampled, and the effects of microstructural features (grain boundaries, dislocations) are more pronounced. With micro-indentation, due to homogeneously distributed micropores and constituent interfaces throughout the composites, hardness values are reduced. Due to the strong influence of pores and interfaces, a direct comparison between nano- and micro-hardness is not carried out here.

Summarizing the homogenised properties measured from individual constituents and the effective properties measured by nanoindentation arrays, the linear rule of mixture provides a good estimation of FG Fe/W composite properties when enough samplings are made (e.g. >25 indents) and pores are excluded.

3.3. Fe—W interface qualification

Microstructural analysis revealed that all composites contain the Fe_7W_6 phase between Fe and W volumes. Hence, the term *Fe—W interface* here describes a collectivity of two interfaces and the Fe_7W_6 phase that exist between the Fe and W volumes, regardless of the heat treatments. The fracture behaviour of the Fe—W interface is investigated using notched micro-cantilever bending tests. An exemplary micro-cantilever, fabricated in the as-sintered 50 W composite with the chevron notch placed within the thin Fe_7W_6 seam is shown in Fig. 2 b). The chevron notch design was chosen so that the crack was forced to initiate at the Fe_7W_6 phase, then followed by its preferred crack path. An example of the load-displacement curve of a chevron-notched micro-cantilever is shown in Fig. 13.

The load-displacement curve first shows elastic deformation, followed by non-linear deformation and then fracture. The fracture load, P_c, is used in Eq. (2) for calculation of fracture toughness. Fig. 14 shows the post-test SEM image of the micro-cantilever. Significant bending of the cantilever and crack growth at the chevron notch were observed, which reflects the non-linear portion of the load-displacement curve. Similar behaviour was also reported by Li et al. in their chevron-notched W-1%Ta micro-cantilevers [48].

Unstable fracture of the shown cantilever occurs at $P_c=0.37$ μN, which is related to the crack deflecting into the bulk material as seen in the dark field TEM image of Fig. 15. This deflection shows a very low energy crack path along an interface. Calculation of fracture toughness should be unaffected by crack deflection as long as the stable-to-unstable transition occurs at the chevron notch. Due to the ex-situ setup used, actual confirmation whether the transition here occurred within the chevron notch, or during the crack deflection, is not possible. However, dimple-like fracture features at the chevron apex shown in Fig. 14 suggest stable crack growth occurred within the chevron notch, followed by unstable fracture, and eventually crack deflection when the crack arrived at the weaker interface outside of the chevron ligament. Based on this interpretation, the effect from crack deflection should be insignificant for the calculation of the fracture toughness for the studied materials.

Using STEM and EDX, three different constituent volumes, Fe, W, and Fe_7W_6, are found in the proximity of the crack. Despite the high dislocation densities and high hardness of Fe, W, and Fe_7W_6, the crack path followed along the interface between the W and Fe_7W_6 volumes. Using Eq. (2), fracture toughness was calculated to be 1.9 MPa $m^{0.5}$. The cantilever fabricated in a 75 W composite aged at 800 °C for 24 h showed the same fracture behaviour and yielded a similar fracture toughness of 1.8 MPa $m^{0.5}$. In contrast, single crystal tungsten micro-cantilevers of similar dimension were more ductile and yielded a value around 6 MPa $m^{0.5}$ [57]. The low toughness is explained here by the complex unit cell structure of Fe_7W_6, which allows only few atom bonds between the W and the Fe_7W_6 lattices, and no coherency. Summarizing the

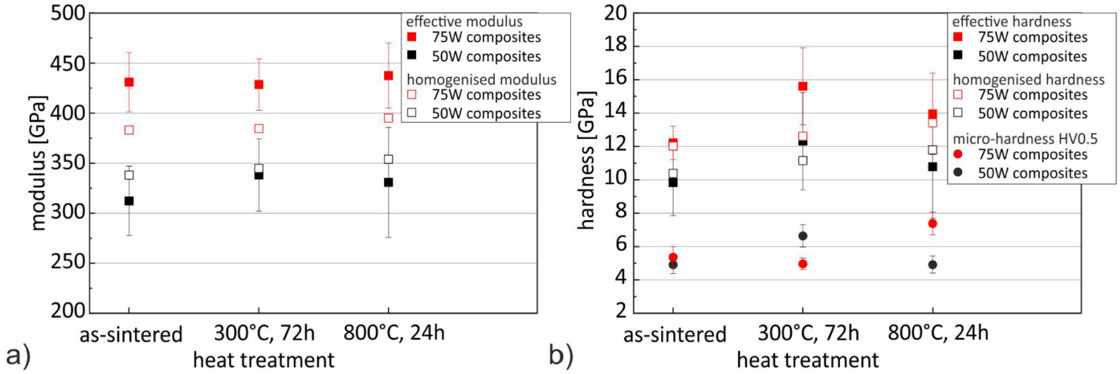

Fig. 12. Results of indentation in 50 W and 75 W composites. a) modulus, b) hardness.Filled rectangles represent the results of measured effective modulus and hardness, empty rectangles represent calculated homogenised results based on the rule of mixture (Eq. (1)), quantitative image analysis (Table 3), and modulus and hardness of individual constituents (Table 4). Additionally, filled circles indicate effective micro-hardness results (HV0.5). Error bars are only given for directly measured effective properties and represent the standard deviation from 25 (nanohardness) and 10 (micro-hardness) indents.

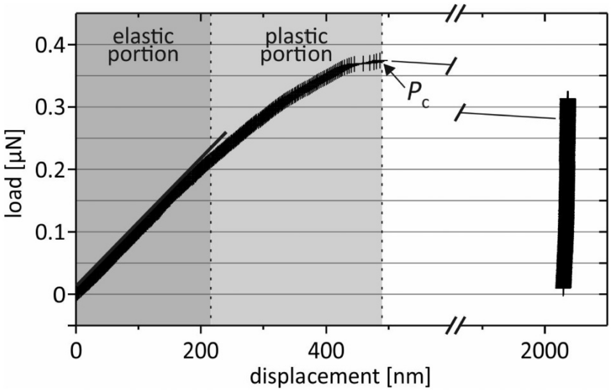

Fig. 13. Exemplary load-displacement curve of a chevron-notched micro-cantilever fabricated in the as-sintered 50 W composite.

toughness observations, the chevron-notched micro-cantilever tests provide an experimental validation of the brittle nature of the Fe/W composites, suggesting that the weak W-Fe_7W_6 interface is contributing to the brittle failure of the Fe/W composite.

4. Conclusion

The present study focusses on the microstructure-to-property relationship of Fe/W composites before and after ageing. The materials are pursued for implementation as graded interlayers in the first wall of future fusion reactors. For this application the materials have to withstand both high temperature for long time and mechanical loads induced from thermal expansion of the adjacent materials. Based on the these requirements, in the present study, the ageing behaviour of ultra-fast sintered Fe/W composites and the mechanical properties of individual constituents are investigated. Homogenised mechanical properties are calculated via a simple rule of mixture and are compared to directly measured effective hardness of the composites.

With respect to application, important aspects concerning properties and behaviour of FG Fe/W composites are found in this study. The hardness of Fe_7W_6, a constituent that is already present in as-sintered composites, was measured to be 17.2 GPa, which is approximately threefold the hardness of of single crystal tungsten [52]. Brittle failure is often associated with high hardness, which is also observed for the other constituents, Fe and W, both exhibiting ultrafine grains and high dislocation densities due to ball-mixing. Despite these conservative results, chevron-notched micro-cantilever bending has identified the interface between Fe_7W_6 and W to be the weakest feature of the composites. Independent from the Fe/W ratio of the composites, this interface shows very low toughness ($K_{\mathrm{Ic}} \approx 1.85$ MPa $\mathrm{m}^{0.5}$) and is suggested as the primary reason for brittle failure of the composites. The observations help explain the high yield strengths and brittle failure of Fe/W composites measured by macroscale four point bending tests in [13]. Ageing experiments have shown that the microstructure of Fe/W composites will change during their application. The amount of Fe_7W_6 will increase along the interfaces between Fe and W volumes on rather short time scales compared to the anticipated first wall life time. Within 72 h at 300 °C, the intermetallic phase already accounts for approximately 30 vol% in the composites. Despite the precipitates' high hardness, the effective modulus and hardness of the composites do not change significantly. Whether the precipitation of Fe_7W_6 during ageing further embrittles the materials requires further discussion, as the most brittle constituent, the Fe_7W_6-W interfaces, is already present in the as-sintered composites. To better understand temperature-induced change of material properties, deeper understanding of the microstructural evolution is required. For the description of temperature- and stress- induced phase transitions in an NiAl alloy, Levitas et al. have developed a multiphase phase field theory [58,59], which is based on the Ginzburg-Landau potential and successfully reflects the microstructural evolution of the NiAl alloy for several temperature and stress scenarios. As their theory allows consideration of multiple phases in a material and can in principle be applied to any phase transformation, the approach may be beneficial in describing the microstructural evolution of the Fe/W composites studied here more systematically in future work. This is particularly interesting as the phase field description allows the calculation of interface stresses between each two phases, which may affect material brittleness. Besides the mathematical description of the microstructural evolution, large-scale mechanical experiments with aged composites will help to understand the influence of precipitates on material properties.

In view of implementation of Fe/W composites in the first wall of fusion reactors as recently discussed, the observed thermodynamic instability, high hardness, and low toughness are not desired. Hence, it is derived that the technique used for production of FG Fe/W interlayers is less relevant than the identification of a thermodynamically more stable material system. An approach that suppresses microstructural changes during reactor operation is required to guarantee long-term applicability.

Considering the techniques used here, chevron-notched micro-cantilevers were recently introduced by Li et al. for the assessment of fracture toughness of brittle and semi-brittle materials [48], and also have proven very efficient for testing the brittle Fe/W composites. The sharp apex and well-defined geometry force a crack to initiate and propagate along a preferred path, which is essential for testing the fracture toughness of the Fe—W interface. Comparing the homogenised modulus and hardness of the composites with effective properties, a reasonably good correlation is achieved when the number of nanoindents for effective property measurement is large enough (>25/composite) and pores are neglected. This proves the hypothesis that the linear rule of mixture can be applied when modelling homogenised modulus and hardness of ideal FG Fe/W layers. This approach has been used in several finite element analyses [5,7,60], however without the

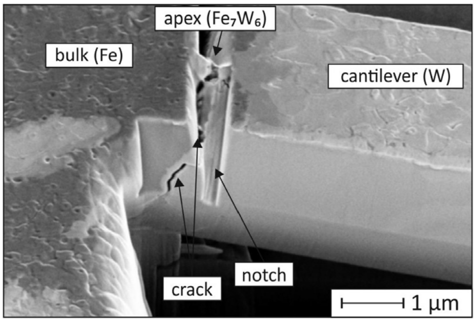

Fig. 14. Exemplary image of a micro-cantilever with chevron-type notch after bending.

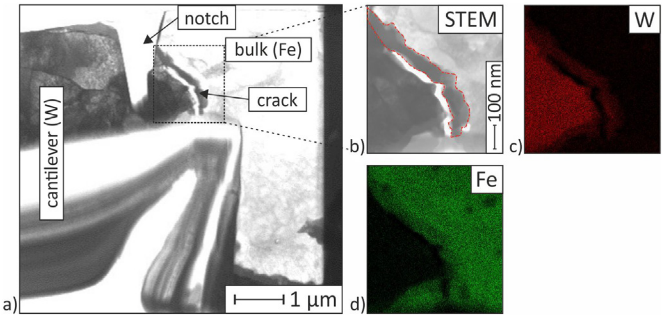

Fig. 15. Detailed image of the crack in the cantilever shown in Fig. 14. a) Overview image of the notch/crack zone, b) STEM image of the crack with the Fe/W mixed volume comprised by a dashed line, c) element map of W in the crack zone, d) element map of Fe. The Fe_7W_6 volume contains ca. 59 at.% Fe and 41 at.% W.

consideration of the influence of Fe_7W_6 and pores. In future work, a more precise estimation may be obtained when taking all constituents and their individual properties into account. Micro-hardness testing, which samples a much larger volume including pores and many interfaces, gave significantly lower hardness than nanoindentation here. The difference is not explained by surface effects in nanoindentation but rather the effect of pores and interfaces. The linear rule of mixture used here and in above finite element studies may not account for their effects, and hence a more comprehensive model will be required in future work to describe the homogenised mechanical properties of actual Fe/W composites.

Data availability

The raw and processed data required to reproduce these findings cannot be shared at this time as the data also forms part of an ongoing study.

CRediT authorship contribution statement

S. Heuer: Conceptualization, Data curation, Formal analysis, Funding acquisition, Investigation, Visualization, Writing - original draft.**B.-S. Li:** Conceptualization, Data curation, Formal analysis, Investigation, Methodology, Validation, Visualization, Writing - original draft.**D.E.J. Armstrong:**Conceptualization, Formal analysis, Funding acquisition, Project administration, Resources, Software, Supervision, Validation, Writing - review & editing.**Y. Zayachuk:**Data curation, Formal analysis, Investigation, Methodology, Writing - review & editing.**Ch. Linsmeier:**Conceptualization, Funding acquisition, Project administration, Resources, Software, Supervision, Validation, Writing - review & editing.

Declaration of competing interest

The authors declare that they have no known competing financial interests or personal relationships that could have appeared to influence the work reported in this paper.

Acknowledgements

This work has been carried out within the framework of the EUROfusion Consortium and has received funding from the Euratom Research and Training Programme 2014–2018 and 2019–2020 under grant agreement no. 633053. The views and opinions expressed herein do not necessarily reflect those of the European Commission. Part of the work was also supported by the Gateway Fellowship programme of the Ruhr-Universität Bochum Research School.

B.-S. Li and D.E.J. Armstrong would like to acknowledge EPSRC Platform Grant EP/P001645/1, EP/R006245/1 and EP/R021775/1 for the financial support.

We are also grateful to Professor Theisen, Chair of Materials Technology of Ruhr-Universität Bochum, Germany, who offered to utilise the Electro Discharge Sinter facility for sample production.

References

[1] P. di Maio, P. Arena, G. Bongiov, P. Chiovaro, R. Forte, S. Garitta, On the optimization of the first wall of the DEMO water-cooled lithium lead outboard breeding blanket equatorial module, Fusion Engineering and Design 109-111 (2016) 335–341, https://doi.org/10.1016/j.fusengdes.2016.02.103.

[2] A. del Nevo, P. Arena, G. Caruso, P. Chiovaro, P. di Maio, M. Eboli, F. Edemetti, N. Forgione, R. Forte, A. Froio, F. Giannetti, G. D. Gironimo, K. Jiang, S. Liu, F. Moro, R. Mozzillo, L. Savoldi, A. Tarallo, M. Tarantino, A. Tassone, M. Utili, R. Villari, R. Zanino, E. Martelli, Recent progress in developing a feasible and integrated conceptual design of the WCLL BB in EUROfusion project, Fusion Engineering and Design doi: https://doi.org/10.1016/j.fusengdes.2019.03.040.

[3] F. A. Hernández, P. Pereslavtsev, G. Zhou, H. Neuberger, J. Rey, Q. Kang, L. V. Boccaccini, E. Bubelis, I. Moscato, D. Dongiovanni, An enhanced, near-term HCPB design as driver blanket for the EU DEMO, Fusion Engineering and Design doi:https://doi.org/10.1016/j.fusengdes.2019.02.037.

[4] W.W. Basuki, R. Dahm, J. Aktaa, Thermomechanical analysis of diffusion-bonded tungsten/EUROFER97 with a vanadium interlayer, J. Nucl. Mater. 455 (1–3) (2014) 635–639, https://doi.org/10.1016/j.jnucmat.2014.09.007.

[5] S. Heuer, T. Weber, G. Pintsuk, J. Coenen, J. Matejicek, C. Linsmeier, Aiming at understanding thermo-mechanical loads in the first wall of DEMO: stress–strain evolution in a Eurofer-tungsten test component featuring a functionally graded interlayer, Fusion Engineering and Design 135 (2018) 141–153, https://doi.org/10.1016/j.fusengdes.2018.07.011.

[6] S. Heuer, J. Coenen, G. Pintsuk, J. Matejícek, M. Vilémová, C. Linsmeier, Overview of challenges and developments in joining tungsten and steel for future fusion reactors, Phys. Scr. (submitted).

[7] D. Qu, W. Basuki, J. Aktaa, Numerical assessment of functionally graded tungsten/EUROFER coating system for first wall applications, Fusion Engineering and Design 98-99 (2015) 1389–1393, https://doi.org/10.1016/j.fusengdes.2015.06.120.

[8] T. Emmerich, D. Qu, R. Vaßen, J. Aktaa, Development of W-coating with functionally graded W/EUROFER-layers for protection of first-wall materials, Fusion Engineering and Design 128 (2018) 58–67, https://doi.org/10.1016/j.fusengdes.2018.01.047.

[9] T. Weber, Development and Optimization of Graded Tungsten/Eurofer97 Joints for Divertor Components (Original Title: Entwicklung Und Optimierung von Gradierten Wolfram/Eurofer97-Verbindungen für Divertorkomponenten), Ph.D. thesis Karlsruher Institut für Technologie, 2012.

[10] T. Weber, M. Stüber, S. Ulrich, R. Vaßen, W. Basuki, J. Lohmiller, W. Sittel, J. Aktaa, Functionally graded vacuum plasma sprayed and magnetron sputtered tungsten/EUROFER97 interlayers for joints in helium-cooled divertor components, J. Nucl. Mater. 436 (1–3) (2013) 29–39, https://doi.org/10.1016/j.jnucmat.2013.01.286.

[11] D. Qu, Z. Zhou, J. Tan, J. Aktaa, Characterization of W/Fe functionally graded materials manufactured by resistance sintering under ultra-high pressure, Fusion Engineering and Design 91 (2015) 21–24, https://doi.org/10.1016/j.fusengdes.2014.12.014.

[12] J. Matějček, B. Nevrlá, M. Vilémová, H. Boldyryeva, Overview of processing technologies for tungsten-steel composites and FGMs for fusion applications, Nukleonika 60 (2) (2015) 267–273, https://doi.org/10.1515/nuka-2015-0049.

[13] S. Heuer, T. Lienig, A. Mohr, T. Weber, G. Pintsuk, J. Coenen, F. Gormann, W. Theisen, C. Linsmeier, Ultra-fast sintered functionally graded Fe/W composites for the first wall of future fusion reactors, Compos. Part B 164 (2019) 205–214, https://doi.org/10.1016/j.compositesb.2018.11.078.

[14] S. Heuer, J. Matějček, M. Vilémová, M. Koller, K. Illkova, J. Veverka, T. Weber, G. Pintsuk, J. Coenen, C. Linsmeier, Atmospheric plasma spraying of functionally graded steel/tungsten layers for the first wall of future fusion reactors, Surf. Coat. Technol. 366 (2019) 170–178, https://doi.org/10.1016/j.surfcoat.2019.03.017.

[15] R. Vaidya, K. Chawla, Thermal expansion of metal-matrix composites, Compos. Sci. Technol. 50 (1) (1994) 13–22, https://doi.org/10.1016/0266-3538(94)90122-8.

[16] D. Hasselman, L.F. Johnson, Effective thermal conductivity of composites with interfacial thermal barrier resistance, J. Compos. Mater. 21 (6) (1987) 508–515, https://doi.org/10.1177/002199838702100602.

[17] P. Gustafson, A thermodynamic evaluation of the C-Fe-W system, Metall. Trans. A. 18 (1987) 175–188.

[18] G. Kostakis, Intermetallic phases of the system Fe-W [Intermetallische Phasen des zweistoffsystems Fe-W], Zeitschrift fuer Metallkunde 76 (1985) 34–36.

[19] B. Koohbor, S. Mallon, A. Kidane, A. Anand, V. Parameswaran, Through thickness elastic profile determination of functionally graded materials, Exp. Mech. 55 (8) (2015) 1427–1440, https://doi.org/10.1007/s11340-015-0043-z.

[20] T. Nakamura, T. Wang, S. Sampath, Determination of properties of graded materials by inverse analysis and instrumented indentation, Acta Mater. 48 (2000) 4293–4306.

[21] G.R. Liu, X. Han, K.Y. Lam, Material characterization of FGM plates using elastic waves and an inverse procedure, J. Compos. Mater. 35 (11) (2001) 954–971, https://doi.org/10.1106/86aq-jy72-5vkt-k1nv.

[22] J. Yu, B. Wu, The inverse of material properties of functionally graded pipes using the dispersion of guided waves and an artificial neural network, NDT & E International 42 (5) (2009) 452–458, https://doi.org/10.1016/j.ndteint.2009.02.006.

[23] R. Butcher, C.-E. Rousseau, H. Tippur, A functionally graded particulate composite: preparation, measurements and failure analysis, Acta Mater. 47 (1) (1998) 259–268, https://doi.org/10.1016/s1359-6454(98)00305-x.

[24] N.A. Branch, N.K. Arakere, G. Subhash, M.A. Klecka, Determination of constitutive response of plastically graded materials, Int. J. Plast. 27 (5) (2011) 728–738, https://doi.org/10.1016/j.ijplas.2010.09.001.

[25] W. Ruigang, P. Wei, J. Mengning, C. Jian, L. Yongming, Investigation of the physical and mechanical properties of hot-pressed machinable si3n4/h-BN composites and FGM, Mater. Sci. Eng. B 90 (3) (2002) 261–268, https://doi.org/10.1016/s0921-5107(01)01048-0.

[26] K. Tohgo, M. Iizuka, H. Araki, Y. Shimamura, Influence of microstructure on fracture toughness distribution in ceramic–metal functionally graded materials, Eng. Fract. Mech. 75 (15) (2008) 4529–4541, https://doi.org/10.1016/j.engfracmech.2008.05.005.

[27] T. Fujii, K. Tohgo, M. Iwao, Y. Shimamura, Fracture toughness distribution of alumina-titanium functionally graded materials fabricated by spark plasma sintering, J. Alloys Compd. 766 (2018) 1–11, https://doi.org/10.1016/j.jallcom.2018.06.304.

[28] F. Erdogan, Fracture mechanics of functionally graded materials, Compos. Eng. 5 (7) (1995) 753–770, https://doi.org/10.1016/0961-9526(95)00029-m.

[29] C.-E. Rousseau, H. Tippur, Dynamic fracture of compositionally graded materials with cracks along the elastic gradient: experiments and analysis, Mech. Mater. 33 (7) (2001) 403–421, https://doi.org/10.1016/s0167-6636(01)00065-5.

[30] N. Jain, A. Shukla, Mixed mode dynamic fracture in particulate reinforced functionally graded materials, Exp. Mech. 46 (2) (2006) 137–154, https://doi.org/10.1007/s11340-006-5867-0.

[31] J. Abanto-Bueno, J. Lambros, An experimental study of mixed mode crack initiation and growth in functionally graded materials, Exp. Mech. 46 (2) (2006) 179–196, https://doi.org/10.1007/s11340-006-6416-6.

[32] A. Kidane, A. Shukla, Quasi-static and dynamic fracture initiation toughness of ti/TiB layered functionally graded material under thermo-mechanical loading, Eng. Fract. Mech. 77 (3) (2010) 479–491, https://doi.org/10.1016/j.engfracmech.2009.10.006.

[33] B. Koohbor, M. Rohanifar, A. Kidane, Characterizing fracture response of cracked transversely graded materials, Compos. Struct. 229 (2019), 111439. https://doi.org/10.1016/j.compstruct.2019.111439.

[34] D. Qu, Development of Functionally Graded Tungsten/Eurofer Coating Systems, Ph. D. thesis Karlsruher Institut für Technologie, 2015.

[35] J. Matějček, H. Boldyryeva, Processing and temperature-dependent properties of plasma-sprayed tungsten–stainless steel composites, Phys. Scr. T138 (2009) 14041, https://doi.org/10.1088/0031-8949/2009/t138/014041.

[36] R. Vaßen, K.-H. Rauwald, O. Guillon, J. Aktaa, T. Weber, H. Back, D. Qu, J. Gibmeier, Vacuum plasma spraying of functionally graded tungsten/EUROFER97 coatings for fusion applications, Fusion Engineering and Design 133 (2018) 148–156, https://doi.org/10.1016/j.fusengdes.2018.06.006.

[37] A. Akbarzadeh, A. Abedini, Z. Chen, Effect of micromechanical models on structural responses of functionally graded plates, Compos. Struct. 119 (2015) 598–609, https://doi.org/10.1016/j.compstruct.2014.09.031.

[38] E. Weissenbek, H. Pettermann, S. Suresh, Elasto-plastic deformation of compositionally graded metal-ceramic composites, Acta Mater. 45 (8) (1997) 3401–3417, https://doi.org/10.1016/s1359-6454(96)00403-x.

[39] J. Yu, A. Kidane, Modeling functionally graded materials containing multiple heterogeneities, Acta Mech. 225 (7) (2013) 1931–1943, https://doi.org/10.1007/s00707-013-1033-9.

[40] S. Schmauder, U. Weber, A. Reuschel, M. Willert, Simulation of the mechanical behaviour of metal matrix composites, Mater. Sci. Forum 678 (2011) 49–60, https://doi.org/10.4028/www.scientific.net/msf.678.49.

[41] J. Matějček, B. Nevrlá, J. Čech, M. Vilémová, V. Klevarová, P. Haušild, Mechanical and thermal properties of individual phases formed in sintered tungsten-steel composites, Acta Phys. Pol. A 128 (4) (2015) 718–721, https://doi.org/10.12693/aphyspola.128.718.

[42] J. Matějček, H. Boldyryeva, V. Brožek, P. Sachr, T. Chráska, Z. Pala, W–steel and w–WC–steel composites and FGMs produced by hot pressing, Fusion Engineering and Design 100 (2015) 364–370, https://doi.org/10.1016/j.fusengdes.2015.06.154.

[43] M. Koller, A. Kruisová, R. Mušálek, J. Matějček, H. Seiner, M. Landa, On the relation between microstructure and elastic constants of tungsten/steel composites fabricated by spark plasma sintering, Fusion Engineering and Design 133 (2018) 51–58, https://doi.org/10.1016/j.fusengdes.2018.05.056.

[44] P. Schütte, Engineering of an Ultra-fast Sintering Device for the Fabrication of Wear-resistant Composite Materials (Original Title: Aufbau einer Kurzzeitsinteranlage zur Herstellung verschleissbestaendiger Verbundwerkstoffe), Ph.D. thesis Ruhr-Universtität Bochum, 2012.

[45] F. Tavassoli, Fusion Demo Interim Design Criteria (DISDC)/Appendix a: Material Design Limit Data/A3.S18E Eurofer Steel, DMN/DIR/NT/2004–000/a, Tech. Rep., DMN Technical Report, 2004.

[46] ITER Materials Properties Handbook (MPH), ITER Doc. G 74 MA 16 04–05-07 R0.1 (Internal Project Document Distributed to the ITER Participants)2017.

[47] D. di Maio, S. Roberts, Measuring fracture toughness of coatings using focused-ion-beam-machined microbeams, J. Mater. Res. 20 (2) (2005) 299–302, https://doi.org/10.1557/jmr.2005.0048.

[48] B.-S. Li, T. J. Marrow, S. G. Roberts, D. E. J. Armstrong, Evaluation of fracture toughness measurements using chevron-notched silicon and tungsten microcantilevers, JOM doi:https://doi.org/10.1007/s11837-019-03696-1.

[49] M.A. Delesse, Procédé mécanique pour déterminer la composition des roches, Ann Des Mines Paris 13 (1848) 379–388.

[50] J. Missiaen, J. Raharijaona, A. Antoni, C. Pascal, M. Richou, P. Magaud, Design of a W/steel functionally graded material for plasma facing components of DEMO, J. Nucl. Mater. 416 (3) (2011) 262–269, https://doi.org/10.1016/j.jnucmat.2011.05.054.

[51] A.-A.F. Tavassoli, A. Alamo, L. Bedel, L. Forest, J.-M. Gentzbittel, J.-W. Rensman, E. Diegele, R. Lindau, M. Schirra, R. Schmitt, H.C. Schneider, C. Petersen, A.-M. Lancha, P. Fernandez, G. Filacchioni, M.F. Maday, K. Mergia, N. Boukos, N. Baluc, P. SpÃ¤tig, E. Alves, E. Lucon, Materials design data for reduced activation martensitic steel type Eurofer, J. Nucl. Mater. 329–333 (2004) 257–262.

[52] Z. Wen, G. Xuanqiao, Z. Pingxiang, H. Zhongwu, L. Laiping, C. Jun, Nanoindentation size effect of tungsten single crystal, Rare Metal Mater. Eng. 46 (12) (2017) 3626–3632, https://doi.org/10.1016/s1875-5372(18)30048-1.

[53] R. Smith, D. Christopher, S. D. Kenny, A. Richter, B. Wolf, Defect generation and pileup of atoms during nanoindentation of Fe single crystals, Phys. Rev. B 67 (24). doi:https://doi.org/10.1103/physrevb.67.245405.

[54] C. Bonnekoh, U. Jäntsch, J. Hoffmann, H. Leiste, A. Hartmaier, D. Weygand, A. Hoffmann, J. Reiser, The brittle-to-ductile transition in cold rolled tungsten plates: impact of crystallographic texture, grain size and dislocation density on the transition temperature, Int. J. Refract. Met. Hard Mater. 78 (2019) 146–163, https://doi.org/10.1016/j.ijrmhm.2018.09.010.

[55] D. Qu, E. Gaganidze, R. Vaßen, J. Aktaa, Determination of W-Eurofer interface toughness at 550C, Eng. Fract. Mech. 202 (2018) 487–499, https://doi.org/10.1016/j.engfracmech.2018.09.016.

[56] C.E. Beck, F. Hofmann, J.K. Eliason, A.A. Maznev, K.A. Nelson, D.E. Armstrong, Correcting for contact area changes in nanoindentation using surface acoustic waves, Scr. Mater. 128 (2017) 83–86, https://doi.org/10.1016/j.scriptamat.2016.09.037.

[57] J. Ast, M. Göken, K. Durst, Size-dependent fracture toughness of tungsten, Acta Mater. 138 (2017) 198–211, https://doi.org/10.1016/j.actamat.2017.07.030.

[58] V. I. Levitas, A. M. Roy, D. L. Preston, Multiple twinning and variant-variant transformations in martensite: phase-field approach, Phys. Rev. B 88 (5). doi:https://doi.org/10.1103/physrevb.88.054113.

[59] V. I. Levitas, A. M. Roy, Multiphase phase field theory for temperature- and stress-induced phase transformations, Phys. Rev. B 91 (17). doi:https://doi.org/10.1103/physrevb.91.174109.

[60] T. Weber, J. Aktaa, Numerical assessment of functionally graded tungsten/steel joints for divertor applications, Fusion Engineering and Design 86 (2–3) (2011) 220–226, https://doi.org/10.1016/j.fusengdes.2010.12.084.